Phycological Society of America

Nanopatterns on silica scales of *Mallomonas* (Chrysophyceae, Stramenopiles): Unraveling UV resistance potential and diverse response to UVA and UVB radiation

Yvonne Nemcova [ID] | Petr Knotek | Iva Jadrná [ID] | Ivana Černajová |
Pavel Škaloud [ID]

Department of Botany, Faculty of Science, Charles University, Prague, Czech Republic

Correspondence
Yvonne Nemcova, Department of Botany, Charles University, Benatska 2, 12800 Prague, Czech Republic.
Email: ynemcova@natur.cuni.cz

Abstract

Mallomonas thrive primarily in freshwaters and dominate plankton communities, especially in oligotrophic waters. The cells have a siliceous cell covering of regularly arranged scales. Despite their ecological importance, the intricate structure and evolutionary significance of their silica scales are still unexplored. We investigated the nanopatterns on the scales and hypothesized that they may play a role in UV shielding. UVA and UVB exposure experiments were performed with 20 *Mallomonas* species, categorized into four groups based on the nanopattern of the scales (plain-scaled, meshed, striated, and papilliferous group); a fifth group consisted of the species that have extremely thick, robust scales regardless of the nanopattern. We revealed that thick scales were associated with enhanced UVB resistance, suggesting a protective role. No significant differences in UVA response were observed among the groups, except for the meshed group, which showed lower resistance, likely due to the less regular pattern on the shield. In conclusion, the scale case, composed of sufficiently silicified scales, provides effective UV protection in freshwater environments, regardless of the particular nanopattern. In increased UVB radiation, the thickness of the scales plays role. Contrary to expectations, cell size and phylogeny do not strongly predict UV resistance. The study highlights the diverse UV responses of *Mallomonas*, but further studies are needed to understand the role of scales/nanopatterns in the ecological adaptations of the species.

KEYWORDS
biosilica, *Mallomonas*, nanopattern, nanostructured biomaterials, normalized growth potential, scales, silica-scaled chrysophytes, ultraviolet radiation, UV exposure

INTRODUCTION

Mallomonas is the most diverse genus within the Synurales (Chrysophyceae, Stramenopiles/SAR), with nearly 200 described species. The genus consists of solitary unicellular flagellates with one or two plastids, one or two visible flagella, and a siliceous cell covering of regularly arranged scales (ca. 2–6 μm). In addition to the scales, most species possess siliceous bristles (Siver, 1991). *Mallomonas* species thrive primarily in freshwaters and dominate plankton communities, especially in oligotrophic waters during the colder season (Siver, 1995). Together with diatoms, chrysophytes are important players in the biogeochemical Si cycling in

---

freshwaters (Lengyel et al., 2023; Marron et al., 2016). The structures consisting of biosilica are formed within the cell in special organelles called silicon deposition vesicles (SDVs). The small-uncharged molecule of silicic acid [Si(OH)4] can diffuse freely across the plasma membrane. However, at low silicic acid concentrations, efficient silicon transporters (group 2 SITs) actively facilitate uptake (Likhoshway et al., 2006; Marron et al., 2016), making silica-scaled chrysophytes successful competitors with diatoms for Si. Moreover, silica-scaled chrysophytes are able to survive under conditions of severe silica depletion that would lead to an brupt decline of the coexisting diatoms (Sandgren et al., 1996).

Unlike diatoms, which produce their silica frustule as a whole during cell division, *Mallomonas* continuously produces scales, scale by scale. The scales are arranged in spirals (Siver & Glew, 1990) so that each scale overlaps the scale behind it in the same row and one or more scales in the upper row (Siver et al., 2013). Hörning et al. (2020) reconstructed the *Mallomonas kalinae* scale-case in silico using 3D data from cryo-FIB scanning electron microscope (SEM) and observed that the number of spirals to the left and right represented consecutive terms in the Fibonacci sequence, similar to those observed in the growth patterns of sunflower seeds, pinecones, or pineapples. So far, however, there have been two theories as to how this patterned arrangement of scales is achieved. Scales are excreted only at a single specific location opposite the flagellum and distributed across a semi-fluid plasma membrane (Lavau et al., 1997), or alternatively, the scales are positioned within SDV beneath the plasma membrane and then inserted subsequently in rows across the entire cell surface (Sandgren et al., 1996).

Scales, composed almost entirely or in combination with silica, are flat to slightly curved plate-like structures with intricate nanopatterns that are used to delineate species taxonomically. All scales possess a base plate that is usually perforated with more or less regularly organized pores and has an upturned rim (Kristiansen, 2002; Siver, 1991). A secondary layer of embedded silica on the base plate is typical for most species. Additional scale structures, present only in some *Mallomonas* species, are the dome and the V-rib. The dome is a raised cavity to which the foot of the bristle is attached. The V-rib originated as an evolutionary novelty in the Early Cretaceous period approximately 111 million years ago, and it is believed to either aid in the spacing and organization of scales forming a scale case (Jo et al., 2013; Siver et al., 2015) or to provide the mechanical stability of the scale (Knotek & Škaloud, 2023) or a combination of both. Although scales are species-specific, they can vary in shape (Neustupa et al., 2010) and ornamentation depending on their final destination on the cell surface. The shape and size of the scales can also be influenced by unfavorable environmental conditions (e.g., pH or temperature) that affect the growth rate of the cells (Nemcova et al., 2010; Nemcova & Pichrtová, 2012; Pichrtová & Nemcova, 2011). Considering the precise overlap of the scales, it is obvious that only a central part of the scale (the shield) and the dome, if present, are exposed to the external environment (Figure 1). The shield is often covered with a unique, species-specific nanopattern that includes, for example, papillae, ribs, or a meshed (reticulated) structure (Figure 2).

So far, we can only speculate about the possible functionality of the chrysophyte siliceous scale case. Conversely, possible adaptive roles of the diatom frustule, which is made of the same material as the chrysophyte scales, have been studied in detail. It was confirmed that the nanopattern on the surface of the diatom frustule affects the movement of particles, thus providing an effective sieve that sorts which particles reach the cell membrane and its receptors. This sorting effect facilitates the uptake of nutrients and silicic acid and prevents the fouling of the cell by colloids and other particles (Hale & Mitchell, 2001). In planktonic species, diatom frustule density, in addition to size and shape, was observed to influence sinking velocity (Miklasz & Denny, 2010). Higher silicification provided stronger mechanical protection and defense against predators and reduced diatom palatability (Hamm et al., 2003; Petrucciani et al., 2022; Xu et al., 2021). Polymerized biosilica of the frustule provided an effective pH buffer that allowed enzymatic conversion of bicarbonate to CO_2 by extracellular carbonic anhydrase (Milligan & Morel, 2002). Increased attention has been paid to distinct aspects of controlling the light regime within the diatom cell. In several centric species, it has been observed that valves are able to collect and concentrate photosynthetically active radiation to intense hotspots just below the cell wall where plastids are concentrated (De Stefano et al., 2007; De Tommasi et al., 2010, 2021; Ferrara et al., 2014; Fuhrmann et al., 2004). The diatom frustule is able to efficiently screen the cell from the ultraviolet (UV) light (Aguirre et al., 2018; De Tommasi et al., 2018; Ellegaard et al., 2016; Su et al., 2018; Zhang et al., 2022). Three mechanisms were revealed by which the frustule protects the living cell from UV: (1) absorption by amorphous porous silica, (2) inhibition of UV collection by diffraction, and (3) wavelength conversion of UV radiation to blue radiation by means of photoluminescent emission (De Tommasi, 2016).

The effects of UV radiation on phytoplankton have been widely documented. Although UVC rays are absorbed by the Earth's ozone layer, UVB radiation can be hazardous or even detrimental, since they affect biomolecules and cellular structures and may interfere with enzymatic reactions and physiological responses such as motility and photoorientation (Häder, 1997; Häder et al., 2015; Karentz et al., 1991; Smith et al., 1992). Absorption of UVB radiation by DNA
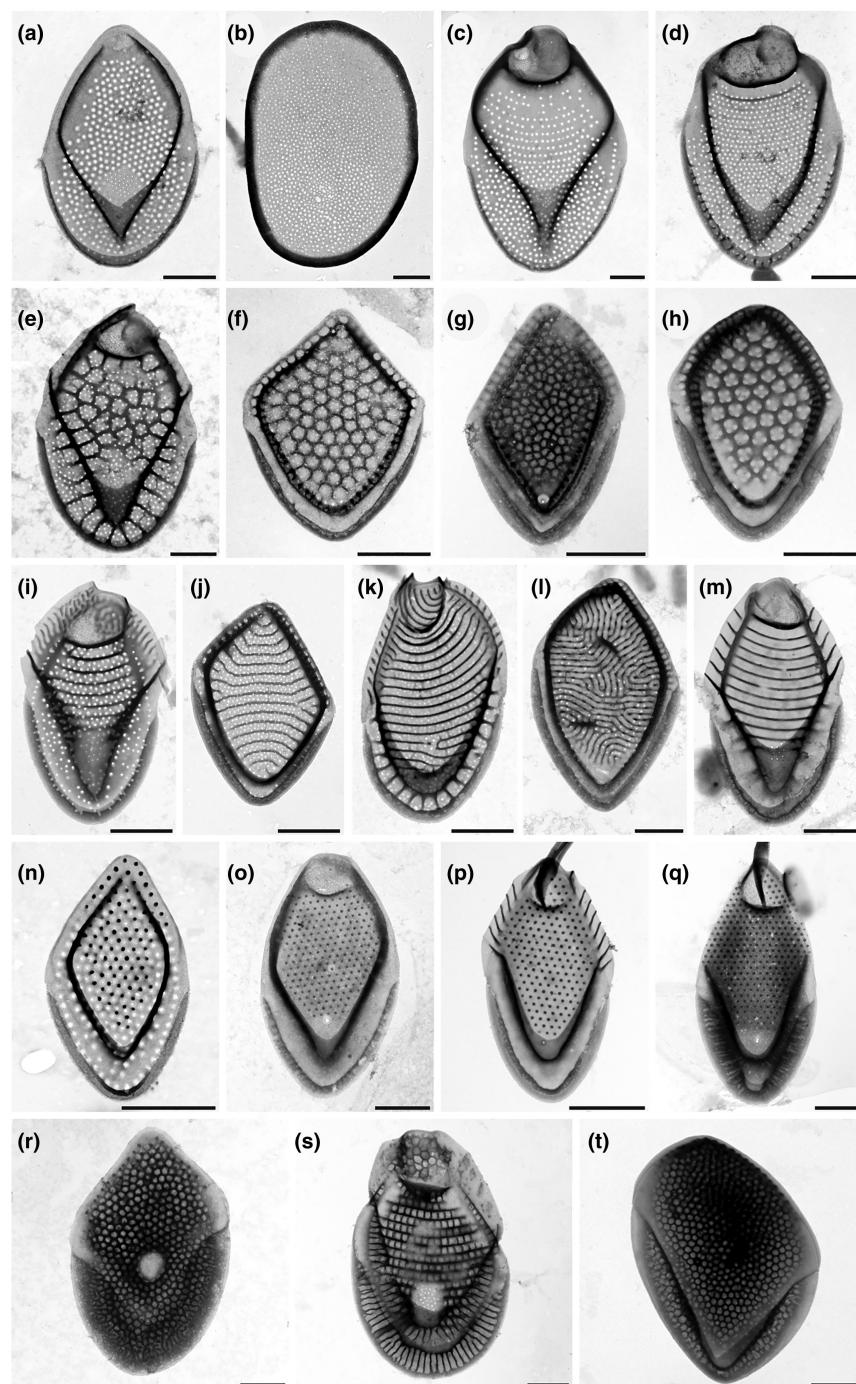
FIGURE 1 Scales of *Mallomonas* species used in UV experiments. (a–d) plain scales. (a) *M. areolata* strain CZ35O. (b) *M. caudata* strain CZ25J. (c) *M. elongata* strain CZ26E. (d) *M. intermedia* strain CZ34M. (e–h) meshed scale-pattern. (e) *M. crassisquama* strain CZ04A. (f) *M. eoa* strain CZ115D. (g) *M. favosa* strain D03C. (h) *M. munda* strain CZ85G. (i–m) striated scale-pattern. (i) *M. actinoloma* var. *maramuresensis* strain CZ105B. (j) *M. doignonii* strain CZ08K. (k) *M. flora* strain CZ53C. (l) *M. schwemmlei* strain CZ33J. (m) *M. striata* var. *striata* strain CZ04D. (n–q) papilliferous scale-pattern. (n) *M. annulata* strain CZ34K. (o) *M. kalinae* strain CCMP479. (p) *M. papillosa* strain CZ03F. (q) *M. rasilis* strain CZ38X. (r–t) thick scales. (r) *M. adamas* strain CZ38K. (s) *M. lelymene* strain CZ29D. (t) *M. splendens* strain AU07B. Bar = 1 μm.

leads to the formation of cyclobutane pyrimidine dimers (CPDs). If CPDs are not repaired, they interfere with base pairing during DNA replication and lead to mutations (Kiefer, 1990). UVA is largely responsible for inhibiting carbon fixation (Bühlmann et al., 1987) and may also induce oxidative DNA damage, including oxidized bases and strand breaks (Cadet et al., 2009). However, UVA may also have beneficial effects on phytoplankton growth, as this radiation is used by the enzyme phytolyase to split UVB-induced CPDs (Häder, 1997).

Based on time-calibrated phylogenies, silica-scaled chrysophytes of the order Synurales originated in the Jurassic approximately 157–163 million years ago (Mya; Čertnerová et al., 2019; Siver et al., 2015). The oldest known record of fossil chrysophyte stomatocysts from a freshwater deposit is known from China and has been dated to the Late Triassic approximately 230 Mya (Zhang et al., 2016). However, these stomatocysts were probably produced by non-scale bearing chrysophytes, as no scales were observed in the sample. Given the lower oxygen content in the atmosphere, consequent less ozone (Lyons et al., 2014), and the fluctuation of solar and cosmic radiation during those geological periods (Shaviv & Veizer, 2003), we

FIGURE 2 Detail of the scale shield exposed to the external environment (a–e); a representative species is given for each group. (a) The plain-scaled group: *Mallomonas elongata* CZ26E. (b) The meshed group: *M. crassisquama* CZ04A. (c) The striated group: *M. flora* CZ54C. (d) The papilliferous group: *M. papillosa* CZ03F. (e) The thick-scaled group: *M. adamas* CZ04D. (f) The whole scale-case of *M. adamas* CZ04D. Bar = 0.5 μm (a–e); Bar = 2 μm (f).
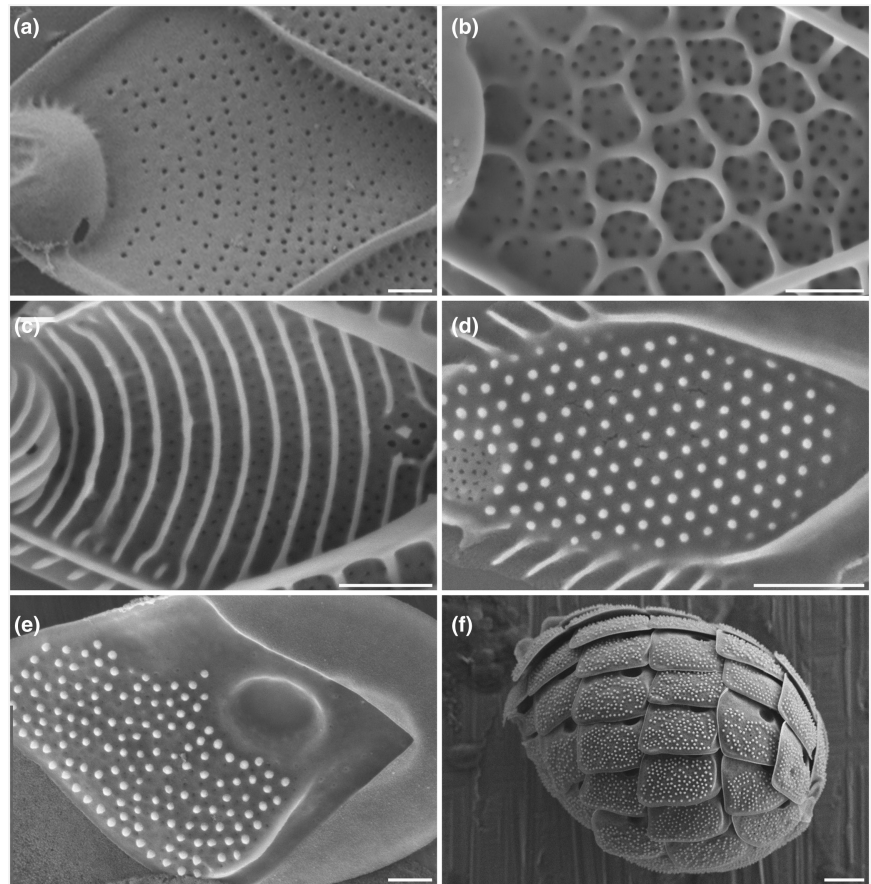
can assume that *Mallomonas* spp. were exposed to varying intensities of ultraviolet radiation during their evolution. One possible function of the *Mallomonas* siliceous scale case is light management of the cell. It can be speculated that the spatial arrangement of the scales interferes with UV optical frequencies, as the physical dimensions of the periodic scale nanopatterns are in order of UV wavelengths (Hörning et al., 2020). However, no UV exposure experiments have been conducted so far. Ellegaard et al. (2016) pointed out that diatoms exhibit a more variable response to UV compared to other algal groups. They suggested as a possible explanation that this variation is due to a species-specific difference in the pattern of pores on the surface of the frustules.

We hypothesized that species-specific nanopattern on the scale shield may lead to variable responses to UVA and UVB in *Mallomonas* spp., and we asked whether some patterns were more effective in UV shielding. Here we report the effects of UVA and UVB exposure on growth rates and survival of 20 *Mallomonas* species, which were divided into four groups based on the scale nanopattern; a fifth group consisted of the species that had extremely thick, robust scales regardless of the nanopattern. We also investigated whether the UV response correlated with cell size or could be influenced by the phylogenetic position of the species.

MATERIALS AND METHODS

Collection, isolation, and cultivation of strains

During 2020, phytoplankton samples were collected from different habitats, mainly on the territory of the Czech Republic, using a 20 μm mesh plankton net. Samples were examined with an Olympus CX 31 light microscope, and individual *Mallomonas* cells were isolated by micropipetting and placed in a 96-well polypropylene plate (Eppendorf microplate 96/F RecoverMax) containing approximately 300 μL of modified liquid WC medium (Boenigk et al., 2006). The medium contained twice the concentration of $Na_2SiO_3 \cdot 9H_2O$ (56.8 mg $\cdot$ L^{-1}) and was buffered with either MES (for CZ115B and CZ115D strains; pH ≈ 6.7) or TES (for the remaining strains; pH ≈ 7.5). After 3–4 weeks, the cultures were inoculated into 25-mL Erlenmeyer flasks filled with the same medium. Two strains (*Mallomonas splendens* CCMP1782 and *M. kalinae* CCMP479) were obtained from the Provasoli-Guillard National Center for Marine Algae and Microbiota (NCMA), and *M. papillosa* Jeongsan121209J was kindly provided by Dr. Woongghi Shin (Chungnam National University). All strains were inoculated and cultivated simultaneously in a cooling box at 14°C, under constant illumination of 50 μmol photons $\cdot$ m^{-2} $\cdot$ s^{-1} (TLD 18 W/33 fluorescent lamps, Philips,

Amsterdam, the Netherlands). Light intensity was measured with a Wallz ULM-500 radiometer equipped with Spherical Micro Quantum Sensor. The strains used in the UV experiments are listed in Table S1 (in the Supporting Information) along with the collection data and authority names. Twenty *Mallomonas* species comprised of 40 strains (two different strains per species) were divided into four groups based on the nanopattern on the shield of the scale: (1) plain scales with pores: *M. areolata, M. caudata, M. elongata,* and *M. intermedia*; (2) scales with meshed or reticulate pattern: *M. crassisquama, M. eoa, M. favosa,* and *M. munda*; (3) striated scales, possessing evenly spaced ribs: *M. actinoloma* var. *maramuresensis, M. doignonii, M. flora, M. schwemmlei,* and *M. striata* var. *striata*; (4) papilliferous scales with regularly spaced papillae: *M. annulata, M. kalinae, M. papillosa,* and *M. rasilis*. A fifth group consisted of the species that have extremely thick, robust scales regardless of the nanopattern: *M. adamas, M. lelymene,* and *M. splendens,* see Figures 1 and 2.

Morphological observation of the cells and silica scales

Live *Mallomonas* cells were observed and photographed using an Olympus BX51 light microscope equipped with Nomarski interference contrast and an Olympus Z5060 camera. For the silica scales observation in a transmission electron microscope (TEM), samples from each culture were dried on Formvar-coated copper grids (SPI Supplies 3220C, West Chester, USA). The grids were rinsed by repeated transfer of the grid in 5 drops of deionized water placed on the hydrophobic surface of a Parafilm strip (PM-996, Bemis, USA). The dried grids were examined using a JEOL 1011 transmission electron microscope (JEOL USA, Inc, Peabody, USA) equipped with a Veleta CCD camera and acquisition software (Olympus Soft Imaging Solution GmbH, Muenster, Germany). For scanning electron microscopy, aliquots of selected cultures were washed by repeated centrifugation in deionized water, air dried on coverslips, attached to aluminum stubs with double-sided adhesive carbon tape, coated with platinum and palladium (4:1) for 95 s using a Bal-Tec SCD 050 sputter coater (Bal-Tec, Balzers, Lichtenstein), and observed with a JEOL Field emission scanning electron microscope JSM-IT800 (JEOL Ltd., Tokyo, Japan). Measurements of cell size were performed on the photographs obtained by light microscopy using ImageJ version Fiji (Schindelin et al., 2012) on at least 20 cells per strain.

Sequencing and phylogenetic analyses

For DNA isolation, ca. 90 mL of well-grown culture were harvested using centrifugation and frozen at 80°C overnight.

Then, genomic DNA was isolated using a DNeasy Blood & Tissue Kit (Quiagen, Venlo, The Netherlands). DNA libraries were prepared using the xGen™ DNA Library Prep EZ UNI Kit, and sequenced on the Illumina NextSeq platform, with 150 bp paired-end reads. Sequenced reads were trimmed with trimmomatic v. 0.32, with the Phred quality scores of 33. De novo assembly of plastid genomes was performed in GetOrganelle v. 1.7.7.0, using *Mallomonas splendens* (NC_040135) and *Synura uvella* (NC_040134) chloroplast genome sequences as seeds. The genomes were assembled using default settings, with different k-mer sizes (21, 45, 65, 85, and 105). Gene prediction was carried out in MFannot (http://megasun.bch.umontreal.ca/apps/mfannot/), and the plastid LSU rDNA, *psa*A, and *rbc*L genes were subtracted for the phylogenetic analysis. Nuclear SSU and LSU rDNA genes were extracted from the trimmed sequenced reads by bwa v. 0.7.3a (Li & Durbin, 2009) using a local alignment of rDNA sequences.

Newly obtained sequences were supplemented by several sequences deposited in the GenBank database. For GenBank accession numbers of genes used in molecular phylogeny see Table S2 (in the Supporting Information). The sequences were aligned using MAFFT version 7 under the Q-INS-I strategy (Katoh & Standley, 2013). DNA alignments are freely available on Mendeley Data: https://doi.org/10.17632/pzrx7sh9vh.1. The loci of nuclear SSU rDNA, nuclear LSU rDNA, plastid LSU rDNA, plastid *rbc*L, and plastid *psa*A genes were concatenated, yielding a robust alignment of 11,382 bases, 96 *Mallomonas* strains, and four outgroup taxa. Prior to performing the concatenated phylogenetic analysis, maximum likelihood (ML) analyses were performed separately for each locus in RAxML 8.1.20 (Stamatakis, 2014) to verify there were no obvious topological incongruencies among the loci. We identified a strong incongruency in the phylogenetic placement of the SSU rDNA gene sequence of *M. torquata* (KM817887) and the *rbc*L gene sequence of *M. adamas* (JQ281502), being inferred as closely related to *M. eoa* and *M. acaroides*, respectively. Since these incongruencies were probably caused by intermixing the strains during the sequencing, we removed the sequences from the alignments. The phylogenetic tree was inferred by Bayesian Inference in MrBayes v3.2.6 (Ronquist et al., 2012) on a concatenated dataset divided into nine partitions (ribosomal genes and codon-partitioned protein-encoded genes), using the GTR + Γ + I evolutionary model. Two parallel Markov chain Monte Carlo (MCMC) runs, with one cold and three heated chains, were run. Trees and parameters were sampled every 100 generations. Convergence of the two cold chains was assessed during the run by calculating the average standard deviation of split frequencies (SDSF). The first 25% of the trees were discarded as burn-in in each run. The bootstrap analysis was performed by ML in RAxML 8.1.20, using

two independent runs, 1000 pseudoreplicates, and the default GTR + Γ evolutionary model.

UV experimental design

Four replicates per strain were inoculated from exponentially growing stock cultures into flat bottom 96-well plates (Eppendorf microplate 96/F RecoverMax) with a starting concentration of 100 F_0 (see below) and a total volume of 125 μL. Four identical sets of plates were prepared (UVA treatment, UVA control, UVB treatment, and UVB control). The UV experiments were performed simultaneously in a cultivation chamber equipped with an extremely efficient cooling system (ProfiRef, Praha, Czech Republic) and provided two independent sections for the UVA and UVB treatments. UV radiation was applied from underneath the well plates resting on the 2-mm-thick JGS2 silicate glass pane that transmits UV radiation (UVS Servis, Praha, Czech Republic). UVA radiation was induced by four narrowband Philips BL PL-L 36W/10 4P fluorescent tubes (with a peak at 380 nm and a maximum intensity of 113.6 W · m^{-2} in the UVA range); UVB was induced by four narrowband Philips PL-L 36W/01/4P fluorescent tubes (with a peak at 311 nm and a maximum intensity of 74.2 W · m^{-2} in the UVB range). Throughout the several pilot experiments, UVA/UVB treatment interval and radiation intensity were adjusted. The primary aim was not to simulate solar radiation but to set the parameters to slow down the growth performance of most strains without killing them. Therefore, the intensity was higher than the cells would experience in today's surface waters. The final UVA/UVB intensity was regulated by inserting additional panes of glass or polypropylene between the well plates and the radiation source. The UVA treatment consisted of 5 h of radiation at an intensity of 72.4 W · m^{-2} · d^{-1}, and for the UVB treatment, radiation at an intensity of 11.6 W · m^{-2} was applied for only 5 min per day in the middle of the illuminated phase.

The intensity of UV radiation was measured by a power-meter monitor PM100D equipped with a flat detection head S120VC (Thorlabs, Newton, USA). To achieve the needed wavelength sensitivity for the respective UV spectral range only, we used additional bandpass filters FGUV11 (transparent in the spectral range from 275 to 375 nm) and 10BPF70-400 (330–470 nm). One set of the well plates in each treatment was covered with a cut-off UV filter foil (Ceiba, Brandys and Labem, Czech Republic) and served as a control. The well plates were illuminated from above with photosynthetically active radiation (PAR) 50 μmol photons · m^{-2} · s^{-1} (14:10 h light:dark cycle), and the temperature of the cultivation chamber was set to approximately 14°C. Both UV treatments started after an adaptation period of 24 h. F_0 was measured every day until the majority of strains reached stationary phase (8–14 days).

Growth rate measurement

Cell abundance was estimated from chlorophyll *a* fluorescence yield (F_0) measured with the closed FluorCam FC 800-C (PSI, Drasov, Czech Republic). Growth was quantified as the area under the log-transformed growth curve (AUC), also known as growth potential, to convey information about both the growth rate and carrying capacity of the culture (Todor et al., 2014). After discarding data from non-growing strains, the data were trimmed to include only days when none of the measured strains decreased in abundance. The final growth potential of each strain was calculated by averaging the AUC values across replicates and normalized to the growth of the control (normalized growth potential). Growth characteristics were calculated in R using the growthcurver package (Sprouffske & Wagner, 2016) with the R script published by Škaloud et al. (2024).

Statistical analyses

Shapiro–Wilk tests were performed to determine the distribution of the growth characteristics and did not show evidence of non-normality (UVA: $W = 0.974$, *p*-value = 0.603; UVB: $W = 0.952$, *p*-value = 0.086). A one-way Analysis of Variance (ANOVA) was used for comparing mean differences of growth characteristics in five species groups (defined based on the nanopattern on the shield of the scale and/or scale thickness). The Wilcoxon signed-rank test was used for pairwise comparisons. Linear regression models were used to analyze the relationship between UV response (expressed as normalized growth potential) and cell size of the respective strains. The tests were regarded significant if $p < 0.05$. To test whether the UV response of species could be influenced by their phylogenetic relatedness, we used Blomberg's *K* as an effect size measure (Münkemüller et al., 2012). This measure relates to the Brownian motion model of trait evolution and is designed to allow comparison of observed values among different phylogenies. *K* values equal to 1 correspond to a Brownian motion model. *K* values greater than 1 indicate a strong phylogenetic signal and that traits are being conserved through the evolutionary time. Alternatively, *K* values closer to zero correspond to a random pattern of evolution (Blomberg et al., 2003). To visualize the phylogenetic signal tests, UV response data were mapped onto the Mallomonas phylogeny using the contMap function (phytools package) in R. All analyses were performed in R (version 4.1.2; R Core Team, 2021), using the packages ggplot2, ggsignif, and phytools (Ahlmann-Eltze & Patil, 2021; Revell, 2012; Wickham, 2016).

RESULTS

Nanopatterns

The cell size of 20 *Mallomonas* species (40 strains) used in UV experiments varied from 9 μm (*M. favosa, M. papillosa*, and *M. munda* were the smallest) to ca. 40 μm for *M. caudata*, with a median cell size about 15 μm (Table S1). The scale-case consisted of about 60–100 scales, usually arranged in rows, with the longitudinal axis of the scales perpendicular to the longitudinal axis of the cell. Most of the species used in the experiments had bristles regularly distributed on the cell surface, with the exceptions of *M. splendens* with 4 bristles on the anterior and posterior sides; *M. munda, M. annulata, M. eoa, M. favosa, M. doignonii*, and *M. schwemmlei* with a cluster of bristles only on the anterior end; and *M. adamas*, which had no bristles at all (Figure 2f). *Mallomonas* species were divided into four groups based on the nanopattern of the scale shield; a fifth group consisted of the species with thick scales. The shield is the part of the scale that is exposed to the external environment and the silica nanopattern may interfere with incident light. (1) The plain-scaled group (Figures 1a–d and 2a) included species with plain scales without a distinct secondary layer (*M. caudata*) or possessing only V-rib (*M. areolata, M. elongata*, and *M. intermedia*). The basal plate of the scale is perforated by more or less regularly arranged pores. In *M. elongata* and *M. intermedia*, the pores form regular transverse rows in the area of the shield. (2) The meshed group contained species with scales reinforced by a secondary layer in the form of a mesh or reticulum (Figures 1e–h and 2b). Although the meshes on the shield of *M. eoa* are almost hexagonal, the regularity of the meshes decreases in *M. crassisquama* and *M. munda* and is more irregular in *M. favosa*. Groups of pores in the basal plate are surrounded by a single mesh each. (3) The striated group included species with striated scales that have evenly spaced usually horizontally oriented ribs (Figures 1i–m and 2c). The pores of the basal plate are mostly irregularly organized, with the exception of *M. striata* var. *striata*, with a single group of pores located within the arms of the V-rib. In *M. doignonii*, the ribs are bifurcated in the middle part of the shield, and *M. schwemmlei* has a fingerprint-like system of semicircular ribs. (4) The papilliferous group contained species with scales covered by regularly spaced papillae (Figures 1n–q and 2d). In *M. annulata* the scale is perforated by irregularly distributed pores, while *M. kalinae, M. papillosa*, and *M. rasilis* have a single large pore in the arms of the V-rib. (5) A thick-scaled group included species with extremely thick, robust scales, regardless of nanopattern (Figures 1r–t and 2e). These scales appear dark on TEM images because the electron beam can hardly pass through them due to the thickness of the scales.

Phylogenetic relationship among *Mallomonas* species

The phylogenetic position of seven taxa, *Mallomonas actinoloma* var. *maramuresensis*, *M. flora*, *M. eoa*, *M. munda*, *M. doignonii*, *M. schwemmlei* and *M. favosa*, was established for the first time (Figure 3). The remaining 13 taxa were inferred in the vicinity of previously sequenced strains of these species. Most pairs of strains belonging to the same species were genetically identical. However, in *M. papillosa*, *M. rasilis*, and *M. striata* var. *striata*, we observed genetic divergence between strains, suggesting the presence of cryptic diversity at the species or population level. The species of the plain-scaled group were inferred in two distinct clades corresponding to the presence or absence of the V-rib. The species of the meshed group were also inferred in two distinct clades. The majority of the species were related to *M. torquata* and *M. mangofera* var. *foveata*. However, *M. crassisquama* was nested within the clade of V-rib-bearing species, which contained mostly plain-scaled species. The species of the striated group were genetically the most diverse. *Mallomonas actinoloma* var. *maramuresensis* was related to the plain-scaled group species; *M. doignonii* and *M. schwemmlei* were related to *M. torquata;* and the remaining two species formed distinct positions in clades that included other striated species, such as *M. asmundiae* and *M. cratis*. Most papilliferous species were inferred as members of the single clade additionally including *M. furtiva*. However, *M. annulata* formed a distinct, unrelated clade, sister to *M. akrokomos*. Finally, the species of the thick-scaled group were placed into two genetically distant clades. Although *M. splendens* and *M. adamas* were related to *M. bronchartiana*, *M. lelymene* formed an independent lineage distantly related to *M. striata* var. *striata* and *M. asmundiae*.

UV exposure experiments

Mallomonas cultures in well plates were exposed to UVA radiation at an intensity of 72.4 W · m^{-2} for 5 h per day and to a UVB radiation pulse at an intensity of 11.6 W · m^{-2} for 5 min per day for 8–14 days (until the strain reached stationary phase). Control cultures were covered with a cut-off UV filter foil. The spectrogram in Figure 4 shows the spectrum measured in the experimental and control cultures as a function of wavelength. It can be seen that the UV radiation is efficiently filtered out from the control cultures.
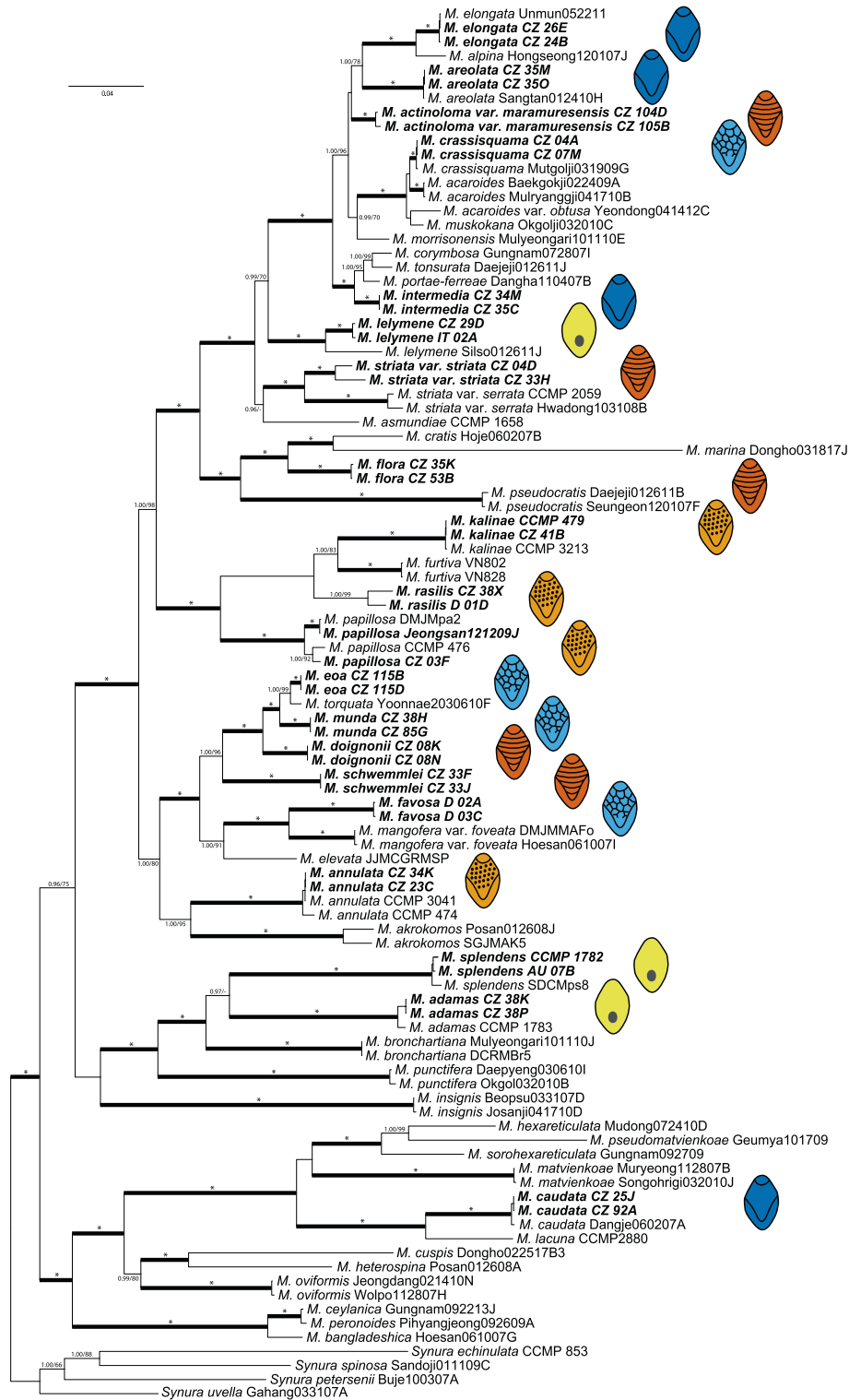
FIGURE 3   Phylogeny of the genus *Mallomonas* obtained by Bayesian inference of the concatenated nuclear SSU and LSU rDNA, and plastid LSU rDNA, *psa*A, and *rbc*L gene datasets. Values at the nodes indicate statistical support estimated by two methods: MrBayes posterior node probability (left) and maximum likelihood bootstrap (right). The nodes receiving the highest statistical supports (1.00/100) are marked with asterisks "*" and thick branches. Newly obtained and sequenced strains are in bold and labeled with a symbol according to their classification into four groups based on the nanopattern on the scale shield; fifth group represents thick-scaled species. Scale bar represents the expected number of substitutions per site. [Color figure can be viewed at wileyonlinelibrary.com]
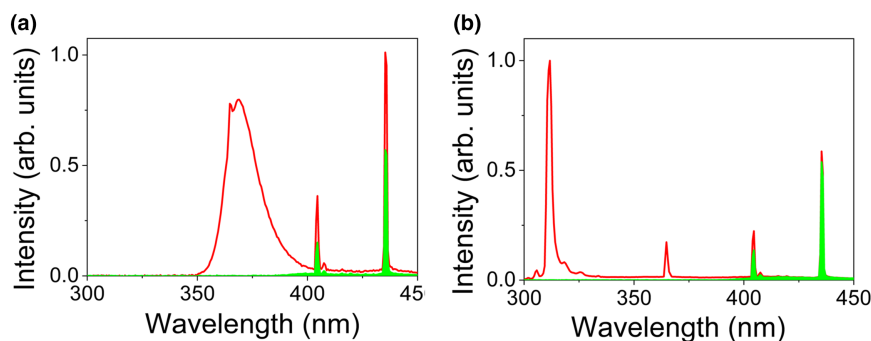
FIGURE 4 Fluorescent tube spectrum measured inside the well plate without (darker line) and with (ligher line) cut-off UV filter foil. Well plate covered with a cut-off UV filter foil served as a control. (a) UVA radiation was induced by a narrowband Philips BL PL-L 36 W/10 4P fluorescent tube. (b) UVB radiation was induced by a narrowband Philips PL-L 36 W/01/4P fluorescent tube. [Color figure can be viewed at wileyonlinelibrary.com]

UVA exposure (Figures 5a and 6a)

The plain-scaled group responded very uniformly to UVA treatment. In the majority of the strains tested, growth potential decreased compared to the control. (On average, normalized growth potential, NGP, decreased by 14%). Only *Mallomonas intermedia* CZ35C performed better under UVA exposure than the control. The meshed group was strongly negatively affected by UVA compared to the other groups, with growth of *M. munda* CZ85G being suppressed the most (61% decrease). The median decrease in NGP was 43%, and none of the strains grew better than the control. In the striated group, there was a relatively broad response to UVA treatment with a median decrease in NGP of 17%. Four strains grew better than the respective control (*M. striata* var. *striata* CZ04D, both strains of *M. doignonii*, CZ08N and CZ08K, and *M. flora* CZ35K). Within the papilliferous group, the UVA response was relatively narrow in the interquartile range, but the whiskers extended over a wider range. The median decrease in NGP was 9%. Both strains of *M. annulata* (CZ34K and CZ23C) grew better than the control. The performance of *M. kalinae* (CCMP479 and CZ41B) was identical to the control. UVA irradiation of *M. papillosa* (Jeongsan121209J) resulted in a 52% decrease in NGP. There was a broad response to UVA radiation in the thick-scaled group (9% median decrease in NGP), with growth enhanced in both strains of *M. adamas* (CZ38K and CZ38P) and suppressed in both strains of *M. lelymene* (CZ29D and CZ38P). The performance of two strains of *M. splendens* differed significantly. *Mallomonas splendens*, strain AU07B grew better, while CCMP1782 grew worse than the control. There was a statistically significant difference between the groups at a 0.05 significance level as determined by one-way ANOVA ($F_{4, 27} = 3.491$, $p = 0.020$). The meshed group was most negatively affected by UVA radiation. At a 0.05 significance level, this group was significantly different from the plain-scaled group ($p = 0.0022$), the striated group ($p = 0.02$), the papilliferous group ($p = 0.0087$), and the thick-scaled group ($p = 0.026$) based on the Wilcoxon signed-rank test.

All other pairwise comparisons were not significantly different.

UVB exposure (Figures 5b and 6b)

All strains in all five groups were severely affected by UVB radiation pulses. None of the strains grew better than the non-irradiated control. The response to UVB treatment was relatively broad in all groups, except for the thick-scaled group. In addition, the response of the two strains within a species was more uniform compared to the UVA treatment. The median decrease in normalized growth potential (NGP) in the plain-scaled group was 71%, with *Mallomonas caudata* CZ25J being the most suppressed (82% decrease in NGP). A median decrease in NGP of 72% was recorded in the meshed group, with *M. crassisquama* CZ04A being the most severely affected (83% decrease in NGP). In contrast, in *M. favosa* D03C, NGP decreased by only 47%. In the striated group, there was a median decrease in NGP of 62%, with *M. flora* CZ35K showing an 85% decrease in NGP. The median decrease in NGP in the papilliferous group was 68%. The group with the highest resistance to repeated UVB irradiation pulses was the thick-scaled group (median decrease in NGP of 40%). A decrease in NGP of <50% was observed in four strains: *M. adamas* CZ38K, *M. adamas* CZ38P, *M. lelymene* CZ38P, and *M. splendens* AU07B (38%, 35%, 38%, and 42% decrease in NGP, respectively). There was a statistically significant difference between the groups as determined by one-way ANOVA ($F_{4, 35} = 6.147$, $p < 0.001$) at the 0.05 significance level. The thick-scaled group was the most resistant to UVB radiation pulses and was significantly different from the plain-scaled group ($p = 0.0027$), the meshed group ($p = 0.008$), the striated group ($p = 0.0075$), and the papilliferous group ($p = 0.00067$) at the 0.05 significance level based on the Wilcoxon signed-rank test. All other pairwise comparisons were not significant. The strains that were more resistant to UVA treatment
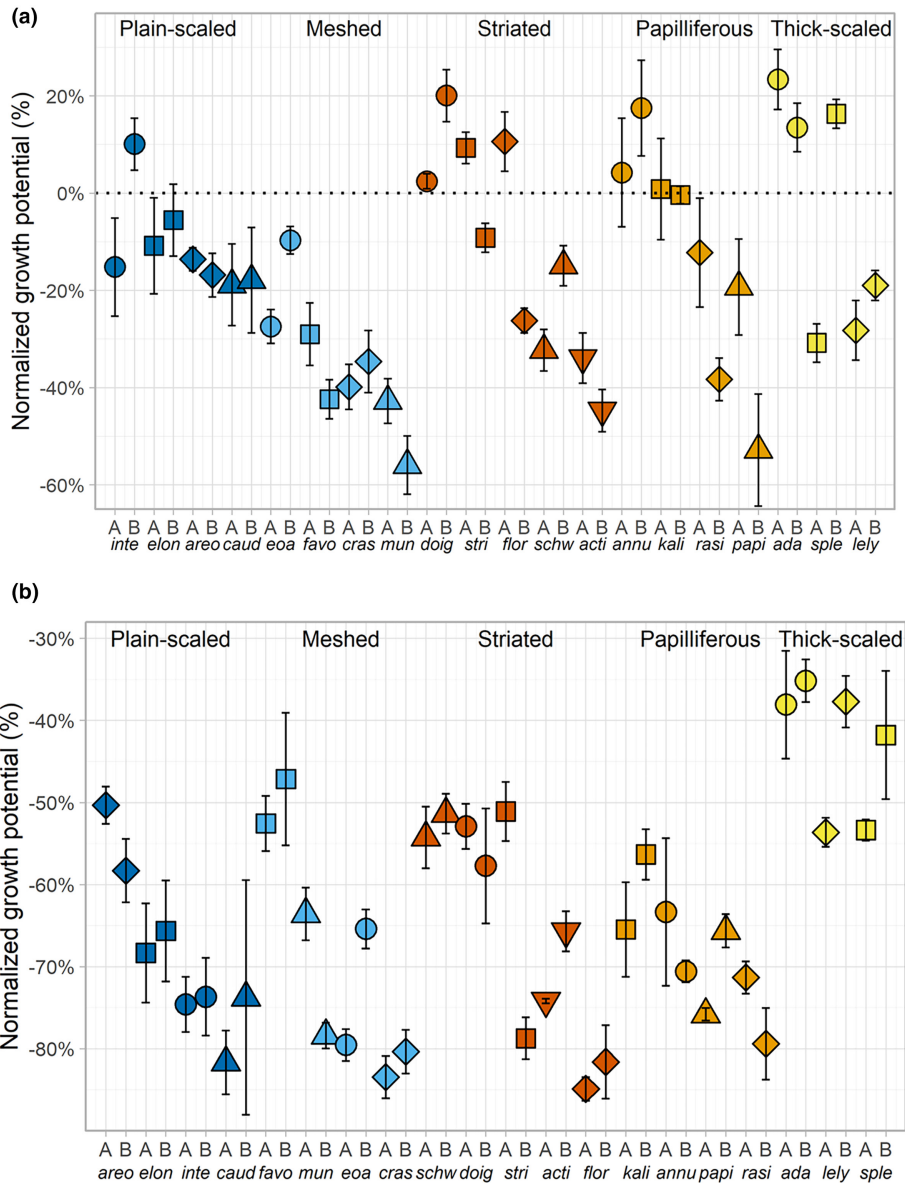
FIGURE 5 Boxplots displaying UV response (expressed as normalized growth potential) across individual *Mallomonas* species based on the nanopattern. Whiskers represent the maximum and minimum values. (a) UVA. (b) UVB. *acti* = *M. actinoloma* var. *maramuresensis*, A: CZ104D, B: CZ105B; *ada* = *M. adamas*, A: CZ38K, B: CZ38P; *annu* = *M. annulata*, A: CZ23C, B: CZ34K; *areo* = *M. areolata*, A: CZ35M, B: CZ35O; *caud* = *M. caudata* A: CZ25J, B: CZ92A; *cras* = *M. crassisquama*, A: CZ04A, B: CZ07M; *doig* = *M. doignonii*, A: CZ08K, B: CZ08N; *elon* = *M. elongata*, A: Strain CZ24B, B: CZ26E; *eoa* = *M. eoa*, A: CZ115B, B: CZ115D; *favo* = *M. favosa*, A: D02A, B: D03C; *flor* = *M. flora*, A: CZ35K, B: CZ53C; *inte* = *M. intermedia*, A: Strain CZ34M, B: Strain CZ35C; *kali* = *M. kalinae*, A: CCMP479, B: CZ41B; *lely* = *M. lelymene*, A: CZ29D, B: CZ38P; *mun* = *M. munda*, A: CZ38H, B: CZ85G; *papi* = *M. papillosa*, A: CZ03F, B: Jeongsan121209J; *rasi* = *M. rasilis*, A: CZ38X, B: D01D; *schw* = *M. schwemmlei*, A: CZ33J, B: CZ33F; *sple* = *M. splendens*, A: CCMP1782, B: AU07B; *stri* = *M. striata* var. *striata*, A: CZ04D, B: CZ33H. [Color figure can be viewed at wileyonlinelibrary.com]

were also more resistant to UVB treatment (Pearson's $r = 0.57$, $p = 0.0001$).

Correlation between UV response and cell size, and phylogenetic signal in UV response

Linear regression models were used to test whether the cell size of each strain predicted its UV response (expressed as normalized growth potential). There was a non-significant relationship between normalized UVB growth potential and cell size ($r^2 = 0.07$, $p = 0.099$). However, there was a very weak relationship between normalized UVA growth potential and cell size ($r^2 = 0.114$, $p = 0.033$). This relationship was driven by two outliers in the cell size of *Mallomonas caudata* (data not shown), which has extremely large cells compared to other species (see Table S1). After removing the outliers, the relationship was no longer significant.
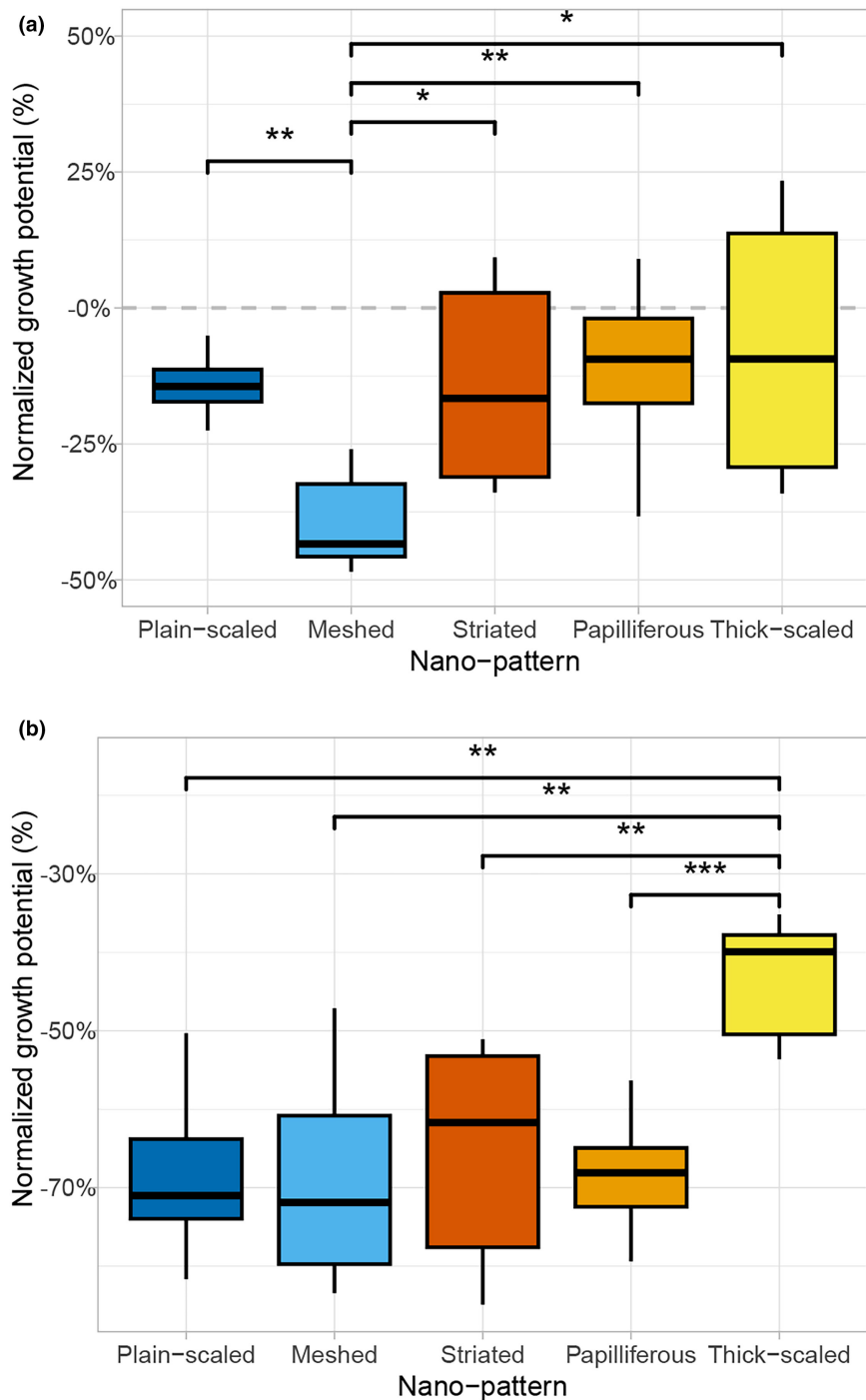
FIGURE 6 Boxplots displaying UV response (expressed as normalized growth potential) across the groups of *Mallomonas* species based on the nanopattern. Whiskers represent the maximum and minimum values, and the bold line within each box represents the median. (a) UVA. (b) UVB. Significance codes: *$p < 0.05$; **$p < 0.01$; ***$p < 0.001$. [Color figure can be viewed at wileyonlinelibrary.com]

We hypothesized that species differences in UV response might reflect phylogenetic signals. To test this, we applied Blomberg's K metrics. For this measure, high phylogenetic signal results from closely related species showing more similarity in a measured trait than species drawn randomly from a given phylogeny. In contrast, a low phylogenetic signal results from a lack of similarity in a measured trait within clades of closely related species (Blomberg et al., 2003). There was no evidence of a high phylogenetic signal for either UVA (Blomberg's $K = 0.009$, $p = 0.009$) or UVB response (Blomberg's $K = 0.011$, $p = 0.001$) indicating high divergence in this trait between closely related species. To visualize the phylogenetic signal for the UVA and UVB response data, each strains' UV response (expressed as NGP) was mapped onto the *Mallomonas* phylogeny (Figure 7a,b). An evolutionary trait map did not show strong divergence in UV response among *Mallomonas* clades.

DISCUSSION

The scale-case of chrysophytes consists of scales covered with a pattern of periodic nanostructures that
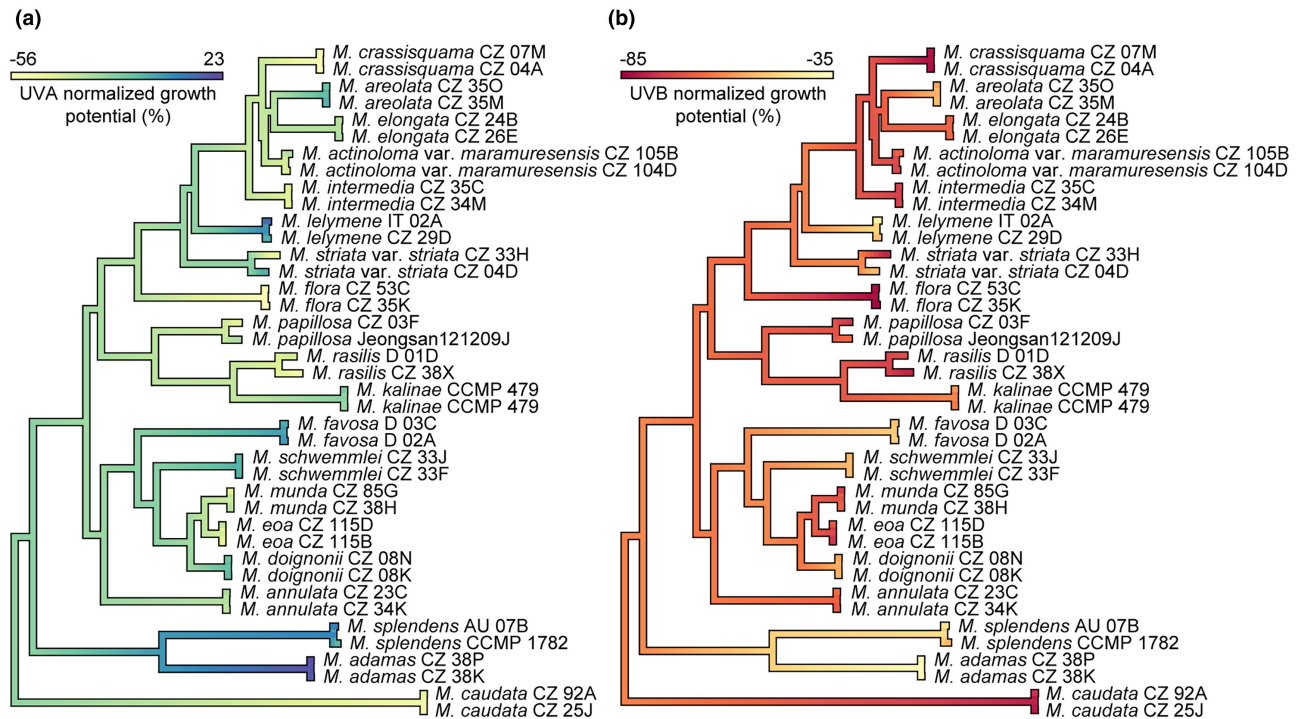
FIGURE 7 Phylogenetic signal tests for UVA and UVB response, mapped on the *Mallomonas* phylogenetic tree. Each tree is colored using the contMap function according to a scale where the darkest color in "a" indicates the maximum values of normalized growth potential (NGP) observed and the darkest color in "b" indicates the minimum NGP values observed. (a) UVA. (b) UVB. [Color figure can be viewed at wileyonlinelibrary.com]

are reproduced in each generation. It was speculated by Hörning et al. (2020) that the arrangement and architecture of the scales might interfere with optical UV frequencies, as the experimentally observed structures are of the order of deep-UV wavelengths. The siliceous covering of chrysophytes is chemically identical to a diatom frustule. Varying effects of UV on cultured diatoms have been observed in terms of response and sensitivity (for a review see Ellegaard et al., 2016). This has raised speculations as to why the differences in UV effects vary more in diatoms than in other algal groups, where the response can usually be correlated with cell size (due to self-shading) and UV-absorbing compounds (for review see Waring et al., 2006). A possible explanation could be that this difference is due to the species-specific pattern of holes or other nanostructures on the frustule (Ellegaard et al., 2016). In this study, we set out to determine if the species-specific nanopattern on the scale shield lead to variable response to UVA and UVB in *Mallomonas* spp., and we asked whether some patterns are more effective in UV shielding. To best of our knowledge, this is the first study exploring the direct effects of UV radiation on the performance of silica-scaled chrysophytes. We also explored how the UV response relates to phylogenetic signal or cell size.

The UV radiation conditions used in this study were more severe than the conditions to which cells are exposed in natural habitats. These conditions resulted from several pilot experiments, and the parameters (intensity and time) were adjusted to slow down the growth performance of most of the 40 strains. It was not our intention to simulate today's solar radiation. Model calculations have shown periodic bursts of increased ultraviolet radiation occurred at the surface during Earth's history, associated with substantial ozone reductions likely due to magnetic polarity transitions (Glassmeier & Vogt, 2010; Reid et al., 1976), so we can assume that silica-scaled chrysophytes were exposed to fluctuating UV intensities during their evolution. Furthermore, natural habitats are exposed to a wide range of radiation in the ultraviolet spectrum, whereas narrowband fluorescent tubes were used in our experiments. Moreover, in natural conditions, UV protection can be enhanced in humic-stained waters, where the strong selective absorbance of shorter wavelengths has been confirmed (Hessen & Van Donk, 1994). In natural habitats, *Mallomonas* can also avoid UV radiation by migrating to deeper water layers. The swimming ability of *Mallomonas* is related to cell size (larger species can swim faster), and diurnal vertical migration of several species has been described (Salonen et al., 2024). However, the ability to avoid UV radiation by vertical migration was very limited in our experiments due to the small volume of the experimental well plate (125 μL). Here we report that at least some *Mallomonas* species are resistant to increased UV radiation, similar to diatoms and terrestrial algae.

All *Mallomonas* strains tolerated prolonged UVA radiation (5 h of radiation at an intensity of 72.4 W · m^{-2} · d^{-1}, with a peak at 380 nm) better than a 5-min UVB pulse (radiation at an intensity of 11.6 W · m^{-2} · d^{-1}, with a peak at 311 nm). The strains that were more resistant to UVA treatment were also more resistant to UVB treatment ($r = 0.57$, $p = 0.0001$), indicating general defense mechanisms against UV. A reduction in normalized growth potential was observed in all strains under UVB treatment. Studies that have investigated the response to UVB radiation over longer periods of time have shown that many phytoplankton species can adapt to this stress, and their growth rates even return to the performance of the control (Hazzard et al., 1997; Zudaire & Roy, 2001). In our study, no adjustment to the repeated UVB pulses was observed (data not shown), although plenty of time (14 h of optimal PAR irradiation) was available daily for light-induced DNA repair. This can probably be explained by the higher intensity of UVB radiation used in our study. The most resistant strain, *Mallomonas adamas* CZ38P, decreased its normalized growth potential by only 38%, while the most sensitive strain, *M. flora* CZ35K, decreased by 85%. This is consistent with the results of Karentz et al. (1991), who studied cell survival after a single UVB pulse in Antarctic diatoms and found a wide range of interspecific UVB sensitivity in the species studied.

Conversely, not all *Mallomonas* strains were negatively affected by regular UVA exposure. Twenty-five percent of the tested strains showed a higher normalized growth potential than the control, although the applied UVA irradiance was higher than at the natural localities. The used narrowband Philips BL PL-L 36W/10 4P fluorescent tube has a peak at 380 nm, which is relatively close to the visible spectrum. It has been shown that low UVA intensity can stimulate carbon fixation and cell division, leading to an increased growth rate in microalgae (Jokiel & York, 1984; Kitzing & Karsten, 2015). These observations have been attributed to increased production of DNA replication enzymes, which are also required for nucleotide excision repair and may be related to the stimulation of photosynthesis (Karentz et al., 1991). More data is needed to determine the cause of the accelerated growth rate at low intensity UVA exposure. However, the biologically effective exposure, which is obtained by weighting spectral irradiance by the appropriate function of wavelength, was about 10 times higher in our UVA experiment than at midday on an unshaded Earth surface (Diffey, 1991). Although, we cannot rule out the presence of UV protectants (e.g., mycosporine-like amino acids) in silica-scaled chrysophytes, we hypothesize that thriving in the increased UVA irradiance is due to the silica scale-case. In diatoms, absorption by the amorphous silica of the frustule has been identified as one of the mechanisms that protect a living cell from UV radiation (Ferrara et al., 2014). Cultures of scaled *Mallomonas* can be transformed into completely naked (scale-less) cells when grown in a silica-depleted medium (Sandgren & Walton, 1995). The scale-less population of *Mallomonas* strains seems ideal to test the role of scales in UV protection in our study. We rejected these experiments because a silica-free environment caused stress to the cells, resulting in suppressed cell division over a prolonged period (Sandgren et al., 1996), and we used growth characteristics as a measure of UV resistance. In diatoms, where the cell cannot exist without a frustule, information on the optical properties leading to UV protection was presumably obtained by experiments on a single cleaned frustule (De Tommasi, 2016). Given the much smaller dimensions of *Mallomonas* silica scales, this would be a challenging approach.

A general relationship between cell size and UV sensitivity has been proposed. Small cells should be more sensitive to UV radiation than large cells because (1) pigment-specific absorption generally increases and internal molecular self-shading decreases in small cells, resulting in higher exposure per unit pigment and cell volume, and (2) the protective efficiency of UVB-absorbing substances is a function of cell size through its effect on molecular self-shading (Garcia-Pichel, 1994). The UV sensitivity of 12 species of Antarctic diatoms was highest in the smaller cells with a larger surface area-to-volume ratio. These smaller cells suffered more damage per DNA unit and were killed by less UVR radiation than the larger cells (Karentz et al., 1991). Contrasting observations were made by Milot-Roy and Vincent (1994), who reported a twofold higher sensitivity of the larger cell fraction to UVR. In our study, no strong correlation was observed between UV response and cell size. There was a weak positive relationship between UVA response and cell size ($r^2 = 0.114$, $p = 0.033$), but this was probably due to outliers in the large *M. caudata* cells. Similarly, Laurion and Vincent (1998) concluded that cell size is not a good predictor of UV sensitivity in natural plankton communities. Other morphological characteristics have been mentioned that influence the transmission of UV light into the cytoplasm of diatoms, for example, the formation of colonies or a canopy of thick setae surrounding the chains of cells in *Chaetoceros* species (Karentz et al., 1991). In *Mallomonas*, four modes of bristle arrangement are known: (1) cells without bristles, (2) cells with bristles attached to scales in the anterior part of the cell, often surrounding a flagellar pore, (3) cells with bristles at both ends, and (4) bristles scatters over the entire surface of the cell (Kristiansen, 2002). In our experiment, however, we did not find a correlation between bristle mode and UV performance (data not shown).

There was no evidence of a strong phylogenetic signal for the UV response, suggesting that common ancestry does not predict differences among the experimental *Mallomonas* species. The divergence of related species was evident when the UV response

was compared in a phylogenetic context (Figure 7a,b). Surprisingly, in *M. flora*, *M. rasilis*, and *M. papillosa*, we observed relatively different UVA responses between two different strains within the same species; we had expected more uniform results based on the same scale ultrastructure (Figures 5a and 7a). In the above species, each strain was isolated at a distinct, spatially and temporally isolated locality. In contrast, when both strains were isolated at the same time in the same location, they showed a more uniform response to UVA (Figure 5a), for example, *M. areolata*, *M. schwemmlei*, *M. eoa*, and *M. doignonii* (see Table S1). It is possible that, at least in some species, other factors related to the original environment (e.g., pigment concentration and composition) influence UVA resistance. There were no major differences in UVB response between strains of the same species (Figure 5b).

After excluding cell size and phylogeny as major drivers of UV resistance, we focused on the silica scales and their species-specific nanopatterns. Species with extremely thick, robust scales, which belonged to the thick-scaled group, were significantly more resistant to the strong UVB pulses compared to the other four groups based on the scale nanopattern (Figure 6b). The scale thickness in *Mallomonas adamas* can be up to 600 nm (Lavau & Wetherbee, 1994) and in *M. splendens* ca. 400–450 nm (Weatherill et al., 2007), which is about 10 times the thickness of other scales; for example, the scales of *M. rasilis* are 50–60 nm thick, with the thickness doubling in the papilla area (Weatherill et al., 2007). *Mallomonas adamas* with a compact scale-case (Figure 2f) was the most resistant species to both UVA and UVB treatments. Increased protection caused by thick scales is in agreement with a study on diatoms, where the overall thickness of the frustule was also a critical factor for UV filtering efficiency (Su et al., 2018). The UVB resistance of all other groups (plain-scaled, meshed, striated, and papilliferous) was not significantly different. No significant difference was observed in UVA response among groups (Figure 6a), with the exception of one group of scales with the reticulated pattern (meshed group) on the shield, which was significantly less resistant. We hypothesize that the mesh pattern is less regular and does not fulfill the characteristics of a lattice-periodic photonic structure as defined by Fuhrmann et al. (2004). The narrow UV response within the plain-scaled and papilliferous groups could be due to the lack of a secondary structure and a regular arrangement of the papillae (vertical, horizontal, and diagonal rows), respectively. A variety of nanopatterns in the striated and meshed groups is probably too diverse to be grouped together, reflecting a broad UV response. Similarly, it has been speculated that the diverse response to UV treatment in diatoms is due to the species-specific pattern of holes or other nanostructures on the frustule (Ellegaard et al., 2016). To evaluate the optical properties and UV shielding capacity (UV transmission and reflection efficiency) of the scale nanopatterns, measurements need to be performed on large-area scale monolayers similar to the monolayers of diatom frustules (Su et al., 2018). Further research is needed to determine whether the single scale can act as a photonic crystal, as has been observed in diatoms. The photonic crystal is defined as a spatial distribution of refractive indexes that, when properly dimensioned, can inhibit propagation of light in specific wavelength ranges (creating photonic band gaps), so depending on dimensions, cells can be screened from UV (Fuhrmann et al., 2004). The question arises whether the spacing and regular organization of papillae, transverse ribs, or reticulated designs in silica scales function similarly to the regularly spaced pores in diatom frustule. Furthermore, the role of base plate pores and their potential interplay with other secondary structures are not known.

We explored the direct effects of UVA and UVB radiation on the performance of 20 species of silica-scaled chrysophytes, revealing diverse responses. Having ruled out cell size and phylogeny as primary factors influencing UV resistance, we focused on the role of silica scales and their species-specific nanopatterns. Similar to diatoms, the thickness of the scales had a remarkable effect on resistance to intense UVB radiation. The group of species with thick scales was the most resistant, regardless of the nanopattern. No significant difference in UVA response was observed among the groups, except for the group with reticulated scales (meshed group), which showed significantly lower resistance, probably due to the less regular pattern on the shield. Some *Mallomonas* strains were even positively affected by regular UVA exposure; about a quarter of the strains tested showed a higher normalized growth potential than the control. We conclude that the scale case, consisting of sufficiently silicified scales, provides effective UV protection in freshwater environments and that the species-specific pattern on the shield of the scale may have other functions, such as strengthening the scales.

AUTHOR CONTRIBUTIONS

ORCID

Yvonne Nemcova https://orcid.org/0000-0002-5396-5717
Iva Jadrná https://orcid.org/0000-0002-2974-536X
Pavel Škaloud https://orcid.org/0000-0003-1201-3290

REFERENCES

Aguirre, L. E., Ouyang, L., Elfwing, A., Hedblom, M., Wulff, A., & Inganäs, O. (2018). Diatom frustules protect DNA from ultraviolet light. *Scientific Reports*, *8*(1), 5138. https://doi.org/10.1038/s41598-018-21810-2

Ahlmann-Eltze, C., & Patil, I. (2021). *Ggsignif: R package for displaying significance brackets for 'ggplot2.'* PsyArxiv. https://doi.org/10.31234/osf.io/7awm6

Blomberg, S. P., Garland, T., & Ives, A. R. (2003). Testing for phylogenetic signal in comparative data: Behavioral traits are more labile. *Evolution*, *57*, 717–745. https://doi.org/10.1111/j.0014-3820.2003.tb00285.x

Boenigk, J., Pfandl, K., & Hansen, P. (2006). Exploring strategies for nanoflagellates living in a wet desert. *Aquatic Microbial Ecology*, *44*, 71–83. https://doi.org/10.3354/ame044071

Bühlmann, B., Bossard, P., & Uehlinger, U. (1987). The influence of longwave ultraviolet radiation (u.v.-A) on the photosynthetic aktivity (^{14}C-assimilation) of phytoplankton. *Journal of Plankton Research*, *9*, 935–943. https://doi.org/10.1093/plankt/9.5.935

Cadet, J., Douki, T., Ravanat, J.-L., & Di Mascio, P. (2009). Sensitized formation of oxidatively generated damage to cellular DNA by UVA radiation. *Photochemical & Photobiological Sciences*, *8*, 903–911. https://doi.org/10.1039/b905343n

Čertnerová, D., Čertner, M., & Škaloud, P. (2019). Molecular phylogeny and evolution of phenotype in silica-scaled chrysophyte genus *Mallomonas*. *Journal of Phycology*, *55*(4), 912–923. https://doi.org/10.1111/jpy.12882

De Stefano, L., Rea, I., Rendina, I., De Stefano, M., & Moretti, L. (2007). Lensless light focusing with the centric marine diatom *Coscinodiscus walesii*. *Optics Express*, *15*, 18082. https://doi.org/10.1364/OE.15.018082

De Tommasi, E. (2016). Light manipulation by single cells: The case of diatoms. *Journal of Spectroscopy*, *2016*, 1–13. https://doi.org/10.1155/2016/2490128

De Tommasi, E., Congestri, R., Dardano, P., De Luca, A. C., Managò, S., Rea, I., & De Stefano, M. (2018). UV-shielding and wavelength conversion by centric diatom nanopatterned frustules. *Scientific Reports*, *8*, 16285. https://doi.org/10.1038/s41598-018-34651-w

De Tommasi, E., Rea, I., Ferrara, M. A., De Stefano, L., De Stefano, M., Al-Handal, A. Y., Stamenković, M., & Wulff, A. (2021). Underwater light manipulation by the benthic diatom *Ctenophora pulchella*: From PAR efficient collection to UVR screening. *Nanomaterials*, *11*, 2855. https://doi.org/10.3390/nano11112855

De Tommasi, E., Rea, I., Mocella, V., Moretti, L., De Stefano, M., Rendina, I., & De Stefano, L. (2010). Multi-wavelength study of light transmitted through a single marine centric diatom. *Optics Express*, *18*, 12203. https://doi.org/10.1364/OE.18.012203

Diffey, B. L. (1991). Solar ultraviolet radiation effects on biological systems. *Physics in Medicine and Biology*, *36*, 299–328. https://doi.org/10.1088/0031-9155/36/3/001

Ellegaard, M., Lenau, T., Lundholm, N., Maibohm, C., Friis, S. M. M., Rottwitt, K., & Su, Y. (2016). The fascinating diatom frustule—Can it play a role for attenuation of UV radiation? *Journal of Applied Phycology*, *28*, 3295–3306. https://doi.org/10.1007/s10811-016-0893-5

Ferrara, M.A., Dardano, P., De Stefano, L., Rea, I., Coppola, G., Rendina, I., Congestri, R., Antonucci, A., De Stefano, M., & De Tommasi, E. (2014). Optical properties of diatom nanostructured biosilica in *Arachnoidiscus* sp: Micro-optics from mother nature. *PLoS ONE*, *9*, e103750. https://doi.org/10.1371/journal.pone.0103750

Fuhrmann, T., Landwehr, S., El Rharbi-Kucki, M., & Sumper, M. (2004). Diatoms as living photonic crystals. *Applied Physics B*, *78*(3–4), 257–260. https://doi.org/10.1007/s00340-004-1419-4

Garcia-Pichel, F. (1994). A model for internal self-shading in planktonic organisms and its implications for the usefulness of ultraviolet sunscreens. *Limnology and Oceanography*, *39*, 1704–1717. https://doi.org/10.4319/lo.1994.39.7.1704

Glassmeier, K.-H., & Vogt, J. (2010). Magnetic polarity transitions and biospheric effects. In G. Hulot, A. Balogh, U. R. Christensen, C. Constable, M. Mandea, & N. Olsen (Eds.), *Terrestrial magnetism* (Vol. *36*, pp. 387–410). Springer. https://doi.org/10.1007/978-1-4419-7955-1_14

Häder, D.-P. (1997). Effects of UV radiation on phytoplankton. In J. G. Jones (Ed.), *Advances in microbial ecology* (Vol. *15*, pp. 1–26). Springer. https://doi.org/10.1007/978-1-4757-9074-0_1

Häder, D.-P., Williamson, C. E., Wängberg, S.-Å., Rautio, M., Rose, K. C., Gao, K., Helbling, E. W., Sinha, R. P., & Worrest, R. (2015). Effects of UV radiation on aquatic ecosystems and interactions with other environmental factors. *Photochemical & Photobiological Sciences*, *14*, 108–126. https://doi.org/10.1039/c4pp90035a

Hale, M., & Mitchell, J. (2001). Functional morphology of diatom frustule microstructures: Hydrodynamic control of Brownian particle diffusion and advection. *Aquatic Microbial Ecology*, *24*, 287–295. https://doi.org/10.3354/ame024287

Hamm, C. E., Merkel, R., Springer, O., Jurkojc, P., Maier, C., Prechtel, K., & Smetacek, V. (2003). Architecture and material properties of diatom shells provide effective mechanical protection. *Nature*, *42*, 841–843. https://doi.org/10.1038/nature01416

Hazzard, C., Lesser, M. P., & Kinzie, R. A. (1997). Effects of ultraviolet radiation on photosynthesis in the subtropical marine diatom, *Chaetoceros gracilis* (Bacillariophyceae). *Journal of Phycology*, *33*, 960–968. https://doi.org/10.1111/j.0022-3646.1997.00960.x

Hessen, D. O., & Van Donk, E. (1994). Effects of UV-radiation of humic water on primary and secondary production. *Water, Air, and Soil Pollution*, *75*, 325–338. https://doi.org/10.1007/BF00482944

Hörning, M., Schertel, A., Schneider, R., Lemloh, M.-L., Schweikert, M. R., & Weiss, I. M. (2020). Mineralized scale patterns on the cell periphery of the chrysophyte *Mallomonas* determined by comparative 3D Cryo-FIB SEM data processing. *Journal of Structural Biology*, *209*, 107403. https://doi.org/10.1016/j.jsb.2019.10.005

Jo, B. Y., Shin, W., Kim, H. S., Siver, P. A., & Andersen, R. A. (2013). Phylogeny of the genus *Mallomonas* (Synurophyceae) and descriptions of five new species on the basis of morphological evidence. *Phycologia*, *52*, 266–278. https://doi.org/10.2216/12-107.1

Jokiel, P. L., & York, R. H. (1984). Importance of ultraviolet radiation in photoinhibition of microalgal growth. *Limnology and Oceanography*, *29*, 192–198. https://doi.org/10.4319/lo.1984.29.1.0192

Karentz, D., Cleaver, J. E., & Mitchell, D. L. (1991). Cell survival characteristics and molecular responses of antarctic phytoplankton to ultraviolet-b radiation. *Journal of Phycology*, *27*, 326–341. https://doi.org/10.1111/j.0022-3646.1991.00326.x

Katoh, K., & Standley, D. M. (2013). Mafft multiple sequence alignment software version 7: Improvements in performance and usability. *Molecular Biology and Evolution*, *30*, 772–780. https://doi.org/10.1093/molbev/mst010

Kiefer, J. (1990). *Biological radiation effects*. Springer. https://doi.org/10.1007/978-3-642-83769-2

Kitzing, C., & Karsten, U. (2015). Effects of UV radiation on optimum quantum yield and sunscreen contents in members of the genera *Interfilum, Klebsormidium, Hormidiella* and *Entransia* (Klebsormidiophyceae, streptophyta). *European Journal of Phycology*, *50*, 279–287. https://doi.org/10.1080/09670262.2015.1031190

Knotek, P., & Škaloud, P. (2023). The effect of patterned structures on the mechanical resistance of microscopic silica scales. *Fottea*, *23*, 190–200. https://doi.org/10.5507/fot.2023.007

Kristiansen, J. (2002). The genus *Mallomonas* (Synurophyceae): A taxonomic survey based on the ultrastructure of silica scales and bristles. *Opera Botanica*, *139*, 1–218.

Laurion, I., & Vincent, W. F. (1998). Cell size versus taxonomic composition as determinants of UV-sensitivity in natural phytoplankton communities. *Limnology and Oceanography*, *43*, 1774–1779. https://doi.org/10.4319/lo.1998.43.8.1774

Lavau, S., Saunders, G. W., & Wetherbee, R. (1997). A phylogenetic analysis of the Synurophyceae using molecular data and scale case morphology. *Journal of Phycology*, *33*, 135–151. https://doi.org/10.1111/j.0022-3646.1997.00135.x

Lavau, S., & Wetherbee, R. (1994). Structure and development of the scale case of *Mallomonas adamas* (Synurophyceae). *Protoplasma*, *181*(1–4), 259–268. https://doi.org/10.1007/BF01666400

Lengyel, E., Barreto, S., Padisák, J., Stenger-Kovács, C., Lázár, D., & Buczkó, K. (2023). Contribution of silica-scaled chrysophytes to ecosystems services: A review. *Hydrobiologia*, *850*, 2735–2756. https://doi.org/10.1007/s10750-022-05075-5

Li, H., & Durbin, R. (2009). Fast and accurate short read alignment with Burrows–Wheeler transform. *Bioinformatics*, *25*, 1754–1760. https://doi.org/10.1093/bioinformatics/btp324

Likhoshway, Y. V., Masyukova, Y. A., Sherbakova, T. A., Petrova, D. P., & Grachev, M. A. (2006). Detection of the gene responsible for silicic acid transport in chrysophycean algae. *Doklady Biological Sciences*, *408*, 256–260. https://doi.org/10.1134/S001249660603015X

Lyons, T. W., Reinhard, C. T., & Planavsky, N. J. (2014). The rise of oxygen in Earth's early ocean and atmosphere. *Nature*, *506*, 307–315. https://doi.org/10.1038/nature13068

Marron, A. O., Ratcliffe, S., Wheeler, G. L., Goldstein, R. E., King, N., Not, F., De Vargas, C., & Richter, D. J. (2016). The evolution of silicon transport in eukaryotes. *Molecular Biology and Evolution*, *33*, 3226–3248. https://doi.org/10.1093/molbev/msw209

Miklasz, K. A., & Denny, M. W. (2010). Diatom sinkings speeds: Improved predictions and insight from a modified Stokes' law. *Limnology and Oceanography*, *55*, 2513–2525. https://doi.org/10.4319/lo.2010.55.6.2513

Milligan, A. J., & Morel, F. M. M. (2002). A proton buffering role for silica in diatoms. *Science*, *297*, 1848–1850. https://doi.org/10.1126/science.1074958

Milot-Roy, V., & Vincent, W. F. (1994). UV radiation effects on photosynthesis: the importance of near-surface thermoclines in a subarctic lake. *Archiv für Hydrobiologie*, *43*, 171–184.

Münkemüller, T., Lavergne, S., Bzeznik, B., Dray, S., Jombart, T., Schiffers, K., & Thuiller, W. (2012). How to measure and test phylogenetic signal. *Methods in Ecology and Evolution*, *3*, 743–756. https://doi.org/10.1111/j.2041-210X.2012.00196.x

Nemcova, Y., Neustupa, J., Kvíderová, J., & Řezáčová-Škaloudová, M. (2010). Morphological plasticity of silica scales of *Synura echinulata* (Synurophyceae) in crossed gradients of light and temperature – A geometric morphometric approach. *Nova Hedwigia. Beihefte*, *136*, 21–32. https://doi.org/10.1127/1438-9134/2010/0136-0021

Nemcova, Y., & Pichrtová, M. (2012). Shape dynamics of silica scales (Chrysophyceae, Stramenopiles) associated with pH. *Fottea*, *12*, 281–291. https://doi.org/10.5507/fot.2012.020

Neustupa, J., Řezáčová-Škaloudová, M., & Nemcova, Y. (2010). Shape variation of the silica-scales of *Mallomonas kalinae* (Mallomonadales, Synurophyceae) in relation to their position on the cell body. *Nova Hedwigia. Beihefte*, *136*, 33–41. https://doi.org/10.1127/1438-9134/2010/0136-0033

Petrucciani, A., Chaerle, P., & Norici, A. (2022). Diatoms versus copepods: Could frustule traits have a role in avoiding predation? *Frontiers in Marine Science*, *8*, 804960. https://doi.org/10.3389/fmars.2021.804960

Pichrtová, M., & Nemcova, Y. (2011). Effect of temperature on size and shape of silica scales in *Synura petersenii* and *Mallomonas tonsurata* (Stramenopiles). *Hydrobiologia*, *673*, 1–11. https://doi.org/10.1007/s10750-011-0743-z

R Core Team. (2021). *R: A Language and Environment for Statistical Computing*. R Foundation for Statistical Computing.

Reid, G. C., Isaksen, I. S. A., Holzer, T. E., & Crutzen, P. J. (1976). Influence of ancient solar-proton events on the evolution of life. *Nature*, *259*, 177–179. https://doi.org/10.1038/259177a0

Revell, L. J. (2012). Phytools: An R package for phylogenetic comparative biology (and other things). *Methods in Ecology and Evolution*, *3*(2), 217–223. https://doi.org/10.1111/j.2041-210X.2011.00169.x

Ronquist, F., Teslenko, M., Van Der Mark, P., Ayres, D. L., Darling, A., Höhna, S., Larget, B., Liu, L., Suchard, M. A., & Huelsenbeck, J. P. (2012). Mrbayes 3.2: Efficient bayesian phylogenetic inference and model choice across a large model space. *Systematic Biology*, *61*, 539–542. https://doi.org/10.1093/sysbio/sys029

Salonen, K., Järvinen, M., Aalto, T., Likolammi, M., Lindblom, V., Münster, U., & Sarvala, J. (2024). Dynamic adaptation of phytoplankton vertical migration to changing grazing and nutrient conditions. *Hydrobiologia*, *851*, 3639–3663. https://doi.org/10.1007/s10750-024-05526-1

Sandgren, C. D., Hall, S. A., & Barlow, S. B. (1996). Siliceous scale production in chrysophyte and synurophyte algae. I. Effects of silica-limited growth on cell silica content, scale morphology,

and the construction of the scale layer of *Synura petersenii*. *Journal of Phycology*, 32, 675–692. https://doi.org/10.1111/j.0022-3646.1996.00675.x

Sandgren, C. D., & Walton, W. E. (1995). The influence of zooplankton herbivory on the biogeography of chrysophyte algae. In C. D. Sandgren, J. P. Smol, & J. Kristiansen (Eds.), *Chrysophyte algae* (1st ed., pp. 269–302). Cambridge University Press. https://doi.org/10.1017/CBO9780511752292.013

Schindelin, J., Arganda-Carreras, I., Frise, E., Kaynig, V., Longair, M., Pietzsch, T., Preibisch, S., Rueden, C., Saalfeld, S., Schmid, B., Tinevez, J.-Y., White, D. J., Hartenstein, V., Eliceiri, K., Tomancak, P., & Cardona, A. (2012). Fiji: An open-source platform for biological-image analysis. *Nature Methods*, 9, 676–682. https://doi.org/10.1038/nmeth.2019

Shaviv, N. J., & Veizer, J. (2003). Celestial driver of Phanerozoic climate? *GSA Today*, 13, 4. https://doi.org/10.1130/1052-5173(2003)013<0004:CDOPC>2.0.CO;2

Siver, P. A. (1991). *The biology of mallomonas*. Springer. https://doi.org/10.1007/978-94-011-3376-0

Siver, P. A. (1995). The distribution of chrysophytes along environmental gradients: Their use as biological indicators. In C. D. Sandgren, J. P. Smol, & J. Kristiansen (Eds.), *Chrysophyte algae* (1st ed., pp. 232–268). Cambridge University Press. https://doi.org/10.1017/CBO9780511752292.012

Siver, P. A., & Glew, J. R. (1990). The arrangement of scales and bristles on *Mallomonas* (Chrysophyceae): A proposed mechanism for the formation of the cell covering. *Canadian Journal of Botany*, 68, 374–380. https://doi.org/10.1139/b90-049

Siver, P. A., Jo, B. Y., Kim, J. I., Shin, W., Lott, A. M., & Wolfe, A. P. (2015). Assessing the evolutionary history of the class Synurophyceae (Heterokonta) using molecular, morphometric, and paleobiological approaches. *American Journal of Botany*, 102, 921–941. https://doi.org/10.3732/ajb.1500004

Siver, P. A., Wolfe, A. P., Rohlf, F. J., Shin, W., & Jo, B. Y. (2013). Combining geometric morphometrics, molecular phylogeny, and micropaleontology to assess evolutionary patterns in *Mallomonas* (Synurophyceae: Heterokontophyta). *Geobiology*, 11, 127–138. https://doi.org/10.1111/gbi.12023

Škaloud, P., Jadrná, I., Dvořák, P., Škvorová, Z., Pusztai, M., Čertnerová, D., Bestová, H., & Rengefors, K. (2024). Rapid diversification of a free-living protist is driven by adaptation to climate and habitat. *Current Biology*, 34(1), 92–105.e6. https://doi.org/10.1016/j.cub.2023.11.046

Smith, R. C., Prézelin, B. B., Baker, K. S., Bidigare, R. R., Boucher, N. P., Coley, T., Karentz, D., MacIntyre, S., Matlick, H. A., Menzies, D., Ondrusek, M., Wan, Z., & Waters, K. J. (1992). Ozone depletion: Ultraviolet radiation and phytoplankton biology in antarctic waters. *Science*, 255, 952–959. https://doi.org/10.1126/science.1546292

Sprouffske, K., & Wagner, A. (2016). Growthcurver: An R package for obtaining interpretable metrics from microbial growth curves. *BMC Bioinformatics*, 17, 172. https://doi.org/10.1186/s12859-016-1016-7

Stamatakis, A. (2014). RAxML version 8: A tool for phylogenetic analysis and post-analysis of large phylogenies. *Bioinformatics*, 30, 1312–1313. https://doi.org/10.1093/bioinformatics/btu033

Su, Y., Lenau, T. A., Gundersen, E., Kirkensgaard, J. J. K., Maibohm, C., Pinti, J., & Ellegaard, M. (2018). The UV filtering potential of drop-casted layers of frustules of three diatom species. *Scientific Reports*, 8, 959. https://doi.org/10.1038/s41598-018-19596-4

Todor, H., Dulmage, K., Gillum, N., Bain, J. R., Muehlbauer, M. J., & Schmid, A. K. (2014). A transcription factor links growth rate and metabolism in the hypersaline adapted archaeon *Halobacterium salinarum*. *Molecular Microbiology*, 93, 1172–1182. https://doi.org/10.1111/mmi.12726

Waring, J., Underwood, G. J. C., & Baker, N. R. (2006). Impact of elevated UV-B radiation on photosynthetic electron transport, primary productivity and carbon allocation in estuarine epipelic diatoms. *Plant, Cell & Environment*, 29, 521–534. https://doi.org/10.1111/j.1365-3040.2005.01429.x

Weatherill, K., Lambiris, I., Pickett-Heaps, J. D., Deane, J. A., & Beech, P. L. (2007). Plastid division in *Mallomonas* (Synurophyceae, Heterokonta). *Journal of Phycology*, 43, 535–541. https://doi.org/10.1111/j.1529-8817.2007.00356.x

Wickham, H. (2016). *Ggplot2: Elegant graphics for data analysis*. Springer-Verlag. https://ggplot2.tidyverse.org

Xu, H., Shi, Z., Zhang, X., Pang, M., Pan, K., & Liu, H. (2021). Diatom frustules with different silica contents affect copepod grazing due to differences in the nanoscale mechanical properties. *Limnology and Oceanography*, 66, 3408–3420. https://doi.org/10.1002/lno.11887

Zhang, W., Yang, H., Xia, X., Xie, L., & Xie, G. (2016). Triassic chrysophyte cyst fossils discovered in the Ordos Basin, China. *Geology*, 44, 1031–1034. https://doi.org/10.1130/G38527.1

Zhang, Y., Shen, W., Li, L., Long, Z., Li, S., Li, T., Wang, Y., Inganäs, O., & Tang, J. (2022). Living diatoms integrate polysaccharide-Eu3+ complex for UV downconversion. *Journal of Materials Research and Technology*, 19, 2774–2780. https://doi.org/10.1016/j.jmrt.2022.05.187

Zudaire, L., & Roy, S. (2001). Photoprotection and long-term acclimation to UV radiation in the marine diatom *Thalassiosira weissflogii*. *Journal of Photochemistry and Photobiology B: Biology*, 62, 26–34. https://doi.org/10.1016/S1011-1344(01)00150-6

SUPPORTING INFORMATION

Additional supporting information can be found online in the Supporting Information section at the end of this article.

Table S1 *Mallomonas* strains in UV experiments including sampling date, GPS coordinates of the collection site, environmental conditions during sampling (t = temperature; c = conductivity), and the cell size measurements (20 cells per strain; *SD* = standard deviation).

Table S2 GenBank accession numbers of genes used in molecular phylogeny.